Experimental and computational studies of water drops falling through model oil with surfactant and subjected to an electric field

Åsmund Ervik*, Svein Magne Hellesø†, Svend Tollak Munkejord† and Bernhard Müller*
* Dept. of Energy and Process Engineering, Norwegian University of Science and Technology, NO-7491 Trondheim, Norway
Email: asmund.ervik@ntnu.no
† SINTEF Energy Research, P.O. Box 4761 Sluppen, NO-7465 Trondheim, Norway

***Abstract*—The behaviour of a single sub-millimetre-size water drop falling through a viscous oil while subjected to an electric field is of fundamental importance to industrial applications such as crude oil electrocoalescers. Detailed studies, both experimental and computational, have been performed previously, but an often challenging issue has been the characterization of the fluids. As numerous authors have noted, it is very difficult to have a perfectly clean water-oil system even for very pure model oils, and the presence of trace chemicals may significantly alter the interface behaviour. In this work, we consider a well-characterized water-oil system where controlled amounts of a surface active agent (Span 80) have been added to the oil. This addition dominates any trace contaminants in the oil, such that the interface behaviour can also be well-characterized. We present the results of experiments and corresponding two-phase-flow simulations of a falling water drop covered in surfactant and subjected to a monopolar square voltage pulse. The results are compared and good agreement is found for surfactant concentrations below the critical micelle concentration.**

6th May 2014

I. Introduction

The study of a single fluid drop falling through some other fluid has a long tradition of study; the physics of raindrops has been debated ever since Aristotle's ideas on the subject in ancient times. Pioneers in this field include Rayleigh, Kelvin, Stokes, Reynolds and Worthington, the latter of whom dedicated most of his career to the study of splashing drops and pioneered the use of flash photography for this purpose.

In spite of such prolonged study, some details elude our understanding still today. This basic phenomenon is also relevant for various industrial applications. In this paper our focus is on sub-millimetre-size water drops falling through a more viscous medium of slightly lower density, i.e. oil, with an eye towards understanding the processes that govern the operation of electrocoalescers used for crude oil processing [1].

In this context, a particular hurdle is the characterization of the two fluids and whether or not the drop surface is clean. To overcome this uncertainty we consider a system where a surface-active agent (Span 80) is added such that it dominates existing impurities. The whole system is then well-characterized in terms of viscosities, densities and interfacial tension as a function of surfactant concentration. We report the outcome of experiments with a falling drop in this fluid system, where in addition a monopolar square voltage pulse is applied to deform the drop. These experiments are compared with two-phase flow simulations where the electric field and the surface-active agent are taken into account.

II. Theory

The equations that govern the two-phase flow system under consideration are the incompressible Navier-Stokes equations:

$$\boldsymbol{\nabla} \cdot \mathbf{u} = 0 \tag{1}$$

$$\frac{\partial \mathbf{u}}{\partial t} + (\mathbf{u} \cdot \boldsymbol{\nabla})\mathbf{u} = -\frac{\boldsymbol{\nabla} p}{\rho} + \frac{\eta}{\rho}\boldsymbol{\nabla}^2 \mathbf{u} + \mathbf{f} \tag{2}$$

The above equations hold for a single fluid, or separately in each fluid for an immiscible two-phase system. Across the interface between the fluids there will be discontinuities in some quantities, e.g. the pressure. These discontinuities are enforced in a sharp manner using the ghost fluid method and the level-set method in the simulations. We will refer to the drop fluid as having properties with subscript $_1$ and the ambient (bulk) fluid as having properties with subscript $_2$.

For the fluids and drop sizes we consider, the Reynolds number will be $\mathrm{Re} \lesssim 1$ such that the flow is laminar. The terminal velocity of a single falling clean drop can then be predicted by the Hadamard-Rybczynski formula [2], [3]

$$\mathbf{v}_{\mathrm{T,HR}} = \frac{2(\rho_1 - \rho_2)\mathbf{g}R^2(\eta_1 + \eta_2)}{3\eta_2(3\eta_1 + 2\eta_2)} \tag{3}$$

while the terminal velocity of a contaminated drop will be closer to that of a falling rigid sphere, predicted by the Stokes formula [4]

$$\mathbf{v}_{\mathrm{T,S}} = \frac{2(\rho_1 - \rho_2)\mathbf{g}R^2}{9\eta_2}. \tag{4}$$

Note that $\mathbf{g}$ is a vector and the resulting velocity vector will have the correct sign for both a falling and rising drop. We note the curious fact that for a given R these velocities can never be equal, as long as the viscosities are both non-zero and finite. This allows an easy way of distinguishing a clean system from a contaminated one. In practice, it is easier to consider a log-log plot of the drag coefficient versus the drop Reynolds number, since both the Stokes theory and the Hadamard-Rybczynski theory predict these values should fall on a straight line, but they predict two different (parallel) lines.

In addition to the fluid flow, an electric field is imposed on the system. In the experiments this is done by applying a monopolar square voltage pulse to plane electrodes at the top and bottom of the fluid chamber. The electric potential Ψ can be calculated from boundary conditions corresponding to the

Table I. IFT BETWEEN WATER AND OIL FOR DIFFERENT SURFACTANT CONCENTRATIONS

Span 80 concentr. [wt%]	Interfacial tension [mN/m]
0.030	10.0
0.020	10.1
0.015	13.9
0.010	18.8
0.001	29.4

voltage on the two electrodes and from the permittivity $\epsilon\epsilon_0$ in the two fluids by a Laplace equation

$$\boldsymbol{\nabla} \cdot (\epsilon\epsilon_0 \boldsymbol{\nabla}\Psi) = 0. \tag{5}$$

This is the simplest model for a conducting drop in a dielectric medium: we assume that both media are perfect dielectrics but with a high permittivity ratio [5].

III. METHODS

A. Experimental methods

The experiments were conducted with brine water drops falling in Marcol 52 oil. The brine water was prepeared by adding 3.5 % (by weight) NaCl to highly purified water. Marcol 52 is a purified mixture of liquid saturated hydrocarbon that has a very low content of surface-active components. Different amounts of the surfactant Span 80 was added to the oil, completly dominating as a surfactant.

The density of water and oil were measured on a DMA 5000 densitymeter from Anton Paar. The vicsocity of the oil was measured using a Anton Paar MCR 102 rheometer. The viscosity of the water was assumed to be identical to established values for sea water. The experiments were conducted at 21.5°C. At this temperature the viscosity and density of the water were 1.03 mPa·s and 1023.6 kg/m^3, respectively, and those of the oil were 12.4 mPa·s and 832.3 kg/m^3, respectively.

The interfacial tension γ between water and oil was measured using a SIGMA 703D tensiometer with a DuNuoy ring. The results for the different amounts of surfactant are given in Table I. The concentration is given in percent by weight, denoted by wt%. These results indicate that the critical micelle concentration for our system is 0.020 wt%. We will restrict ourselves to concentrations below this.

The experiment consisted of letting water drops fall in the 15 mm gap between an upper and a lower horizontal electrode. A monopolar square voltage was applied to the lower electrode, creating an electrical field $\mathbf{E}$ that distorted the drop. The voltage was generated using a Stanford Research DS340 signal generator connected to a TREK 2020B high voltage amplifier. Field strengths were varied between 266.7 V/mm and 666.7 V/mm for different cases, as given in the following. A side view of the experimental setup is shown in Fig. 1.

A high-speed Cheetah CL near infrared camera with a Infinity KS2 long-range microscope lens was used to record movies of the drops as they fell and were deformed by the field. The camera had a resolution of 640×512 pixels and could record 1730 frames per second. The position and deformation of the drops were extracted from the movies using the Spotlight image analysis software [6]. In particular, the vertical velocity and the ratio of the major and minor axis a/b were determined,

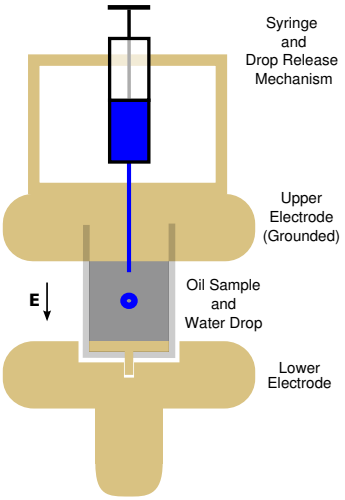

Figure 1. Side view of the experimental setup. The electric field is aligned with the gravitational field.

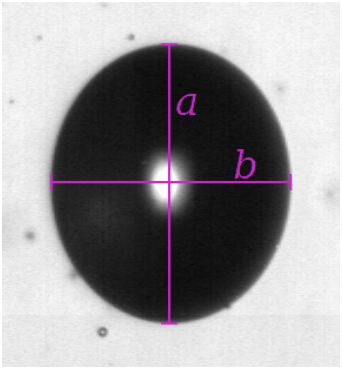

Figure 2. Example of image captured of elongated drop with major and minor axes a and b superimposed.

as shown in Fig. 2 where a slightly elongated water drop is seen with the axes superimposed.

The experimental procedure consisted of these steps:
1. Create a water drop of the desired size at the tip of the glass needle using the screw-in plunger. The field of view of the camera is at the needle tip.
2. Once a drop is created, move the test cell such that the field of view of the camera is at the center of the electrode gap.
3. Arm the camera to start recording on trigger.
4. Release the drop from the tip of the glass needle.
5. Once the drop comes into view of the camera, trigger the camera and voltage source.
6. The camera records a movie of the drop.
7. Extract the drop position and shape from the recorded movie.

B. Simulation and numerical methods

The Navier-Stokes equations (1) and (2) are solved numerically using an in-house code. All reported simulations are done using 2D axisymmetry. The equations are discretized with a finite-difference method, specifically WENO [7] for the convective terms and central differences for the viscous terms. The time integration is done with an explicit Runge-Kutta method (SSPRK (2,2) in the terminology of Gottlieb et

al. [8]). A standard projection method [9] is used to determine the pressure field such the velocity field is solenoidal, giving a Poisson equation for the pressure p. The solution of this Poisson equation demands the majority of the computing time; it is solved here using the Bi-Conjugate Gradient Stabilized method [10] with the BoomerAMG preconditioner [11]. The same methods are used to solve the Laplace equation for the electric field. We employ the PETSc and Hypre libraries for these methods [12], [13].

As stated, the Navier-Stokes equations are valid in each phase separately. The interface between the phases is tracked using the level-set method, see [14] and references therein for a thorough description of how we employ this method. To couple the two phases, the ghost-fluid method (GFM) [15], [16] is used in the simulations to enforce the jumps in different quantities (like pressure) across the interface:

$$[\![\mathbf{u}]\!] = 0, \tag{6}$$

$$[\![p]\!] = 2[\![\eta]\!]\mathbf{n}\cdot\boldsymbol{\nabla}\mathbf{u}\cdot\mathbf{n} + \mathbf{n}\cdot[\![\mathbf{M}]\!]\cdot\mathbf{n} + \gamma\kappa, \tag{7}$$

$$[\![\boldsymbol{\nabla} p]\!] = 0, \tag{8}$$

$$[\![\Psi]\!] = 0, \tag{9}$$

$$[\![\epsilon\mathbf{n}\cdot\boldsymbol{\nabla}\Psi]\!] = 0. \tag{10}$$

$$\begin{aligned}[\![\eta\boldsymbol{\nabla}\mathbf{u}]\!] = [\![\eta]\!]\Big(&(\mathbf{n}\cdot\boldsymbol{\nabla}\mathbf{u}\cdot\mathbf{n})\mathbf{nn} + (\mathbf{n}\cdot\boldsymbol{\nabla}\mathbf{u}\cdot\mathbf{t})\mathbf{nt} \\ &+ (\mathbf{n}\cdot\boldsymbol{\nabla}\mathbf{u}\cdot\mathbf{t})\mathbf{tn} + (\mathbf{t}\cdot\boldsymbol{\nabla}\mathbf{u}\cdot\mathbf{t})\mathbf{tt}\Big) \\ &+ (t\cdot[\![\mathbf{M}]\!]\cdot\mathbf{n}) + \mathbf{tn}(\mathbf{t}\cdot\boldsymbol{\nabla}_\iota\gamma)\mathbf{tn},\end{aligned} \tag{11}$$

Here ι denotes the interface between the two fluids (so $\boldsymbol{\nabla}_\iota$ is the gradient along the interface) and $\mathbf{M}$ is the Maxwell stress tensor calculated from the electric field $\mathbf{E}$. This is again calculated from the potential Ψ which we obtain by solving (5) numerically. With the same approximation as in (5), the Maxwell stress tensor is

$$\mathbf{M} = \epsilon\epsilon_0\Big(\mathbf{EE} - \frac{1}{2}(\mathbf{E}\cdot\mathbf{E})\mathbf{I}\Big), \tag{12}$$

and $\mathbf{n}$ and $\mathbf{t}$ are the normal and tangent vectors to the interface, and formulas like $\mathbf{nn}$ and $\boldsymbol{\nabla}\mathbf{u}$ denote tensors formed by the outer product. Our convention is that the normal vector points out from a drop and that the jump $[\![\cdot]\!]$ is the difference going from the outside to the inside, e.g. $[\![\eta]\!] = \eta_2 - \eta_1$.

This formulation takes into account the pressure difference due to interfacial tension γ in (7), the applied electric field, and the Marangoni effect that arises from an interfacial tension gradient along the interface in (11). The surfactant concentration ξ determines γ through the Langmuir equation

$$\gamma(\xi) = \gamma_0\left(1 + \beta\ln(1 - \frac{\xi}{\xi_\infty})\right); \tag{13}$$

where $\beta = RT\xi_\infty/\gamma_0$ is the interfacial elasticity and ξ_∞ is the maximum possible concentration of surfactant. We consider here an insoluble surfactant which has zero concentration away from the interface. Furthermore, we restrict ourselves to surfactant concentrations which are below the critical micelle concentration (0.02 wt% for our system). An insoluble surfactant is then a good approximation when both the bulk and the interface Peclet numbers, $\mathrm{Pe}_2 = \mathbf{v}_\mathrm{T}\mathrm{R}/\mathrm{D}_{\xi,2}$ and $\mathrm{Pe}_\iota = \mathbf{v}_\mathrm{T}\mathrm{R}/\mathrm{D}_{\xi,\iota}$, are high [17]. Here $\mathbf{v}_T$ is the terminal velocity and $D_{\xi,2}, D_{\xi,\iota}$ are diffusion constants for the surfactant in the bulk phase and on the interface, respectively. There is only sparse literature data on these diffusion constants, but they seem to be around 10^{-10} m/s^2 [18]. We will assume here that the two diffusion constants (and thus the Peclet numbers) are equal, writing simply D_ξ. Tests revealed that our simulations are not very sensitive to the value, with values of 10^{-10} and $5\cdot10^{-7}$ giving indistinguishable results, so a value of 10^{-10} was subsequently used. We may understand this low sensitivity when we compute the respective Peclet numbers, they are 250 and 50 000 for these values of the diffusion constant, which are both $\gg 1$. This indicates that an insoluble surfactant should be a good approximation.

The surfactant is transported along the interface according to an advection-diffusion equation which can be expressed in the same coordinates as all the other equations, by using the curvature of the interface κ and the normal vector $\mathbf{n}$,

$$\begin{aligned}\frac{d\xi}{dt} + \mathbf{u}\cdot\boldsymbol{\nabla}\xi - \mathbf{n}\cdot\boldsymbol{\nabla}\mathbf{u}\cdot\mathbf{n}\,\xi = \\ D_\xi\Big(\boldsymbol{\nabla}^2\xi - \mathbf{n}\cdot\boldsymbol{\nabla}\boldsymbol{\nabla}\cdot\mathbf{n}\,\xi + \kappa(\mathbf{n}\cdot\boldsymbol{\nabla}\xi)\Big),\end{aligned} \tag{14}$$

where the first two terms on the left-hand side and the first term on the right-hand side are the ordinary terms in an advection-diffusion equation, and the remaining terms constitute the restriction of this equation to the interface.

The surfactant transport equation, as well as the level-set equations for interface tracking, are discretized with finite-difference methods and integrated in time using explicit Runge-Kutta methods. We refer to Teigen et al. [16], [19], [20] for a thorough discussion and validation of these models.

IV. Results

A. Terminal velocity

As a consistency check, experimental results for the terminal velocity of falling drops were compared with the theoretical values for drops with and without a surface covering. This was done for several drop diameters and surfactant concentrations, the results are shown in Fig. 3 (unfilled symbols). As this figure shows, the results fall on or close to the line for a solid sphere, which is as expected for a surfactant-covered drop. The dotted line shows the theoretical result for a drop with circulation according to the Hadamard-Rybczynski theory.

Some results from simulations of falling drops are also shown, using the same shapes but with filled symbols. The points plotted in green are simulations with surfactant-covered drops. These were done for a 1329 μm drop in 0.001 wt% Span 80 and for a 859 μm drop in 0.015 wt% Span 80. The points plotted in magenta are equivalent simulations without a surfactant present. It is seen that simulations without surfactant agree well with the Hadamard-Rybczynski theory, while simulations with surfactant agree well with the Stokes theory and with the experimental results.

These simulations were done with a $20R\times40R$ computational domain and a grid resolution of 400×800. Grid refinement studies indicated that this was sufficient. A moving grid procedure was employed, such that the drop was always close to the center of the domain. The simulations were performed using the "laboratory" reference frame, where all velocities approach zero at the boundary conditions, which were identical on all sides of the domain. That is to say, full

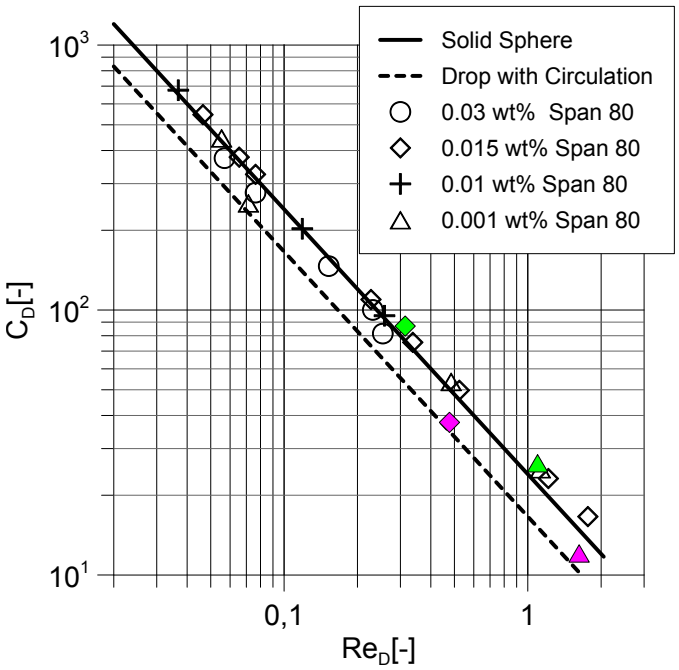

Figure 3. Plot of the drag coefficient versus Reynolds number. Unfilled symbols indicate experimental results. Filled green symbols indicate simulations with surfactant. Filled magenta symbols indicate equivalent simulations without surfactant.

Table II. CASES STUDIED FOR DROP OSCILLATION

Case	Diameter [μm]	Span 80 [wt%]	Field [V/mm]
1	958	0.015	400.0
2	826	0.015	533.3
3	804	0.015	666.7
4	560	0.015	266.7
5	783	0.001	400.0

slip (zero gradient) was used for the tangential velocity while the normal velocity (through the boundaries) was set to zero.

B. Drop deformation

Several experiments were performed with different drop diameters, field strengths and surfactant concentrations. The parameters for each case are summarized in Table II. The drop shapes were extracted from the movies of the experiments using the Spotlight software. The ratio between the major axis a and the minor axis b could then be determined. Analysis of the various uncertainties that affected the measurements a and b was done according to the procedure described in [21], and the uncertainty in a/b was then computed assuming Gaussian error propagation. Herein, the fluid properties were assumed to be without error. This gave a relative error in a/b that was independent of a/b but dependent on the initial radius. The relative error was 2.0 % for the largest drops considered here and 3.4 % for the smallest.

Based on these experiments, equivalent simulations were set up and run. The values of a/b were also extracted from the simulation results, such that they could be plotted and compared directly to the experimental results. Such plots are shown in in Figs. 4 to 8. As is seen in these plots, the agreement between simulations and experiments is good for a variety of parameters. Error bars are shown for the experimental values for every fifth point. The static deformation predicted by the Taylor theory [22] is shown with blue lines at the right-hand side. For Case 1 it is seen that this line agrees very well with the static deformation predicted by simulations without surfactant, thus it overpredicts the deformation in the presence of surfactant.

Note that for Case 3 (Fig. 6), the deformation is much larger so the scale is different. Since the Taylor theory is only valid for small deformations, it has not been applied here. For this case there is some disagreement between experiments and simulations regarding the maximum deformation and for the static deformation. This is likely due to the assumption of insoluble surfactant in the simulation: as the drop is stretched to such a large deformation, the interfacial area increases and there is room for more surfactant at the interface. Thus adsorption kinetics can become important in this case, making the simulations underpredict the deformation.

For Case 2 (Fig. 5) there is also a poor agreement. The cause of this is harder to identify, since the other similar cases gave good agreement. For this case, the difference between experiments and the Taylor theory is also much larger than for the other cases. Further investigations are needed to clarify this point.

For Case 1 (Fig. 4) a plot is also shown for a simulation without surfactant, but using the experimentally measured value for the interfacial tension at 0.015 wt% Span 80 (magenta curve). It is seen that this simulation overpredicts both the initial oscillation and the static deformation. This indicates that the Marangoni forces due to the surfactant are important both for the maximum and the static deformation.

In these simulations the grid resolution was 241×482 in the radial and axial directions, respectively. Simulations using coarser grids indicated that this resolution was sufficient. All simulations were done in axisymmetric coordinates, corresponding to a plane intersecting half the drop. Initial simulations were performed with falling drops that had reached terminal velocity before the field was applied. These were compared with simulations done with a field applied to a drop in zero gravity in a quiescent ambient fluid, and it was found that the difference in deformation was small. Since the initial simulation with the falling drop reaching terminal velocity has a runtime of many days, subsequent drop deformation simulations were done for drops in zero gravity.

For these simulations without gravity, the full domain was $8R\times16R$. The boundary conditions used were identical on all sides of the domain, namely full slip (zero gradient) for the tangential velocity while the normal velocity (through the boundaries) was set to zero. The pressure boundary condition is zero gradient in the normal direction, i.e. $\partial p/\partial \mathbf{n} = 0$.

A detailed view of the simulation result from Case 1 is shown in Fig. 9. The axisymmetric solution is shown mirrored about the symmetry axis (y-axis). The drop is at its most extended. The terminal velocity has been subtracted from the velocity field, such that it appears in the drop reference frame. The orange colour indicates the pressure field and the green color shows the surfactant distribution. The vectors on the right-hand side show the velocity field, and the field lines on the left-hand side show the electric field. A reference vector for

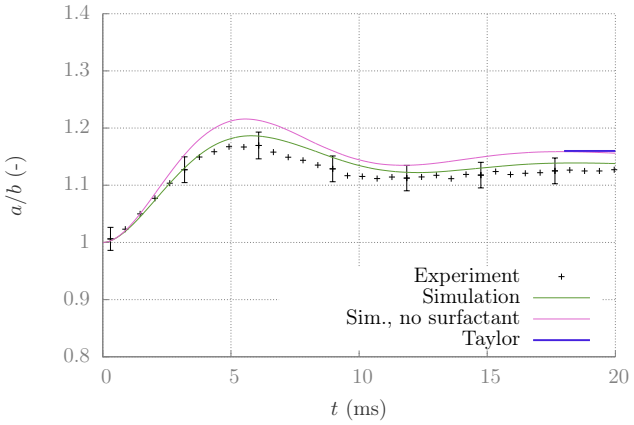

Figure 4. **Case 1:** Simulation and experimental results for the 958 μm water drop falling through Marcol with 0.015 wt% Span 80 subjected to a 400.0 V/mm field

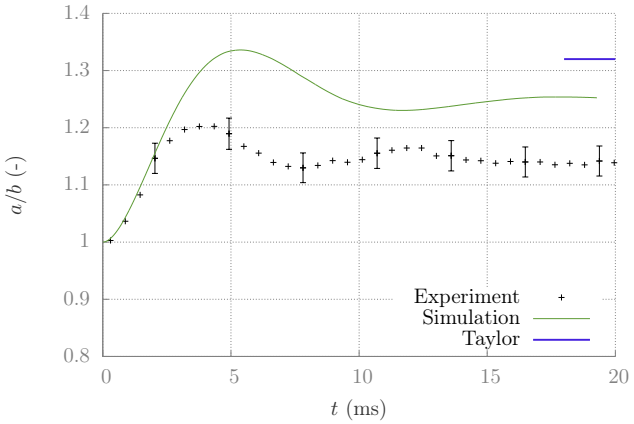

Figure 5. **Case 2:** Simulation and experimental results for the 826 μm water drop falling through Marcol with 0.015 wt% Span 80 subjected to a 533.3 V/mm field

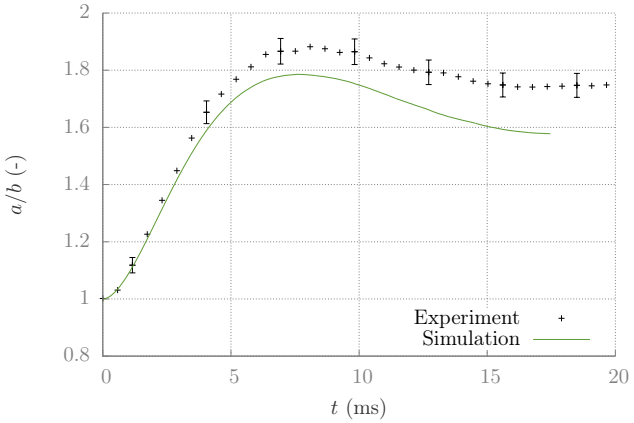

Figure 6. **Case 3:** *Note: different scale!* Simulation and experimental results for the 804 μm water drop falling through Marcol with 0.015 wt% Span 80 subjected to a 666.7 V/mm field

the velocity is shown in the lower right corner. The simulation domain was significantly larger than the view shown.

From this figure it is seen that the velocity field inside the droplet is almost vanishing. This is reasonable, since the

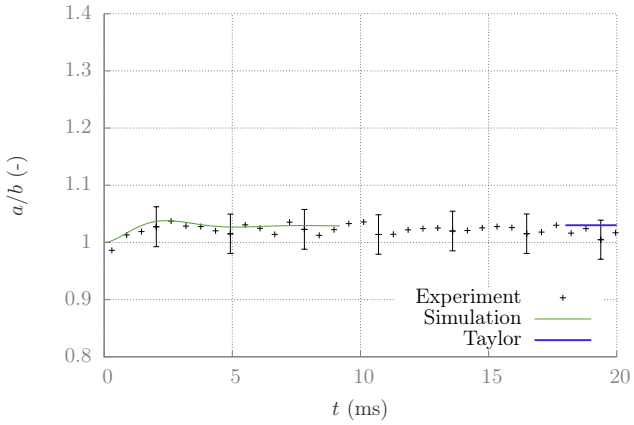

Figure 7. **Case 4:** Simulation and experimental results for the 560 μm water drop falling through Marcol with 0.015 wt% Span 80 subjected to a 266.7 V/mm field

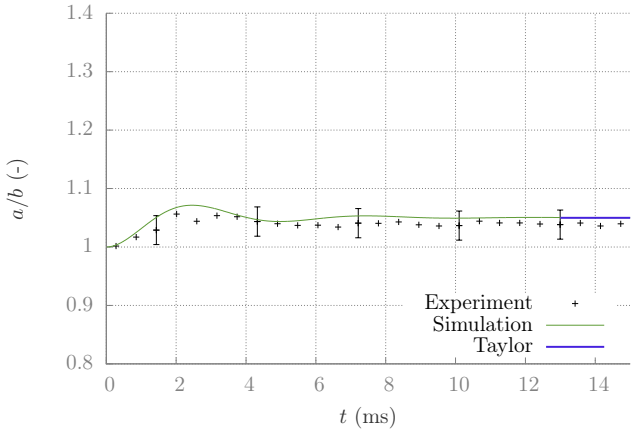

Figure 8. **Case 5:** Simulation and experimental results for the 783 μm water drop falling through Marcol with 0.001 wt% Span 80 subjected to a 400.0 V/mm field

velocity field must be close to zero as it reverses direction. It is also seen that the surfactant distribution is slightly non-uniform, giving rise to Marangoni forces that counteract the velocity field tangential to the interface. The electric field lines shown on the left-hand side pass straight through the droplet, which has high conductivity, and otherwise appear as one would expect.

V. Conclusions

By experiments and computations we have investigated the behaviour of single water drops in Marcol model oil with added surfactant subjected to an electric field. This system is well-characterized in terms of bulk, drop and interface properties. In particular, the terminal velocity and the response to a sudden step in the electric field have been studied.

In our computations, the details of the two-phase flow are captured using the level-set method, and the interfacial jumps are accounted for using the ghost-fluid method (GFM). The surfactant is modelled as insoluble and the fluids are assumed to be perfect dielectrics. The calculated terminal velocities for a clean system agree well with the predictions of the Hadamard-Rybczynski formula. When the presence of surfactant is accounted for, the calculated terminal velocities agree well with the experimentally observed ones, which again

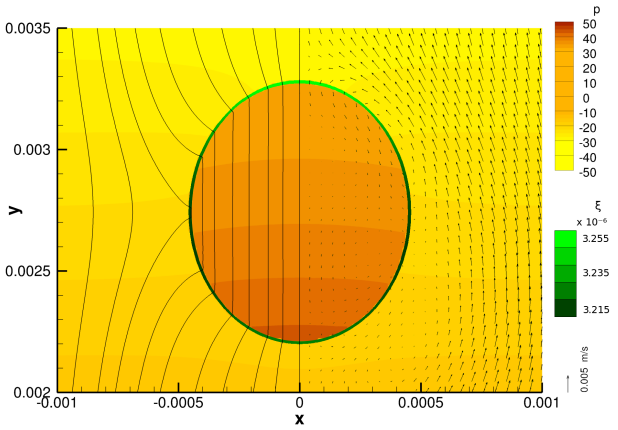

Figure 9. Detailed snapshot from the simulation of Case 1, the drop shown at its greatest extension. On the left-hand side, electric field lines are shown. The orange color shows the pressure field. The green colour on the interface shows the surfactant concentration; the maximum concentration ξ_∞ is $4.18{\cdot}10^{-6}$ for this case.

agree with those calculated using the Stokes formula for rigid bodies.

Our calculations of the dynamic drop stretching as a response to a step change in the electric field agree well with the laboratory observations (except for one case). Our results indicate that it is necessary to account for the presence and dynamics of surfactant in order to reproduce the dynamic behaviour of the drop.

ACKNOWLEDGMENTS

We would like to thank Dr. Martin Fossen (SINTEF Petroleum Research) for the measurements of interfacial tension as a function of surfactant concentration, Dr. Velaug Myrseth Oltedal (SINTEF Petroleum Research) for the measurements of bulk viscosity, and Dr. Cédric Lesaint (SINTEF Energy Research) for the measurements of density. We are also grateful to Dr. Pierre Atten and Prof. Jean-Luc Reboud (G2ELab) and Dr. Erik Bjørklund (Wärtsilä) for fruitful discussions around the work presented here.

This work was funded by the project *Fundamental understanding of electrocoalescence in heavy crude oils* coordinated by SINTEF Energy Research. The authors acknowledge the support from the Petromaks programme of the Research Council of Norway (206976), Petrobras, Statoil and Wärtsilä Oil & Gas Systems.

REFERENCES

[1] J. S. Eow, M. Ghadiri, A. O. Sharif, and T. J. Williams, "Electrostatic enhancement of coalescence of water droplets in oil: a review of the current understanding," *Chem. Eng. J.*, vol. 84, no. 3, pp. 173–192, 2001.

[2] J. Hadamard, "Mouvement permanent lent d'une sphere liquide et visqueuse dans un liquide visqueux," *CR Acad. Sci*, vol. 152, no. 25, pp. 1735–1738, 1911.

[3] W. Rybzynski, "Über die fortschreitende Bewegung einer flüssigen Kugel in einem zähen Medium," *Bull. Acad. Sci. Cracovie*, 1911.

[4] H. Lamb, *Hydrodynamics*, 6th ed. New York: Dover, 1945.

[5] J. Melcher and G. Taylor, "Electrohydrodynamics: a review of the role of interfacial shear stresses," *Ann. Rev. Fluid Mech.*, vol. 1, no. 1, pp. 111–146, 1969.

[6] R. Klimek and T. Wright, *Spotlight-8 Image Analysis Software*, NASA, http://hdl.handle.net/2060/20060011194.

[7] X.-D. Liu, S. Osher, and T. Chan, "Weighted essentially non-oscillatory schemes," *J. Comput. Phys.*, vol. 115, no. 1, pp. 200–212, 1994.

[8] S. Gottlieb, D. I. Ketcheson, and C.-W. Shu, "High order strong stability preserving time discretizations," *J. Sci. Comput.*, vol. 38, no. 3, pp. 251–289, 2009.

[9] A. J. Chorin, "Numerical solution of the Navier-Stokes equations," *Math. Comput.*, vol. 22, no. 104, pp. 745–762, 1968.

[10] H. van der Vorst, "Bi-CGSTAB: A fast and smoothly converging variant of Bi-CG for the solution of nonsymmetric linear systems," *SIAM J. Sci. Comput.*, vol. 13, no. 2, pp. 631–644, 1992.

[11] V. E. Henson and U. M. Yang, "BoomerAMG: a parallel algebraic multigrid solver and preconditioner," *Appl. Numer. Math.*, vol. 41, pp. 155–177, 2000.

[12] S. Balay, W. D. Gropp, L. C. McInnes, and B. F. Smith, "Efficient management of parallelism in object-oriented numerical software libraries," in *Modern Software Tools for Scientific Computing*. Springer, 1997, pp. 163–202.

[13] *hypre: High Performance Preconditioners*, Lawrence Livermore National Laboratory, http://www.llnl.gov/CASC/hypre/.

[14] Å. Ervik, K. Y. Lervåg, and S. T. Munkejord, "A robust method for calculating interface curvature and normal vectors using an extracted local level set," *J. Comput. Phys.*, vol. 257, pp. 259–277, 2014.

[15] R. Fedkiw and X.-D. Liu, "The ghost fluid method for viscous flows," *Progress in Numerical Solutions of Partial Differential Equations, France. Arachon*, 1998.

[16] K. E. Teigen, K. Y. Lervåg, and S. T. Munkejord, "Sharp interface simulations of surfactant-covered drops in electric fields," in *Fifth European Conference on Computational Fluid Dynamics, ECCOMAS CFD 2010*.

[17] S. Sadhal and R. E. Johnson, "Stokes flow past bubbles and drops partially coated with thin films. Part 1. Stagnant cap of surfactant film–exact solution," *J. Fluid Mech.*, vol. 126, pp. 237–250, 1983.

[18] X. Wang, "Characterization of surfactant adsorption at a liquid-liquid interface by drop volume tensiometry," Master's thesis, Concordia University, Canada, 1997.

[19] K. E. Teigen and S. T. Munkejord, "Influence of surfactant on drop deformation in an electric field," *Phys. Fluids*, vol. 22, no. 11, Nov. 2010, article 112104.

[20] K. E. T. Giljarhus and S. T. Munkejord, "Numerical investigation of electrostatically enhanced coalescence of two drops in a flow field," in *Dielectric Liquids (ICDL), 2011 IEEE International Conference on*. IEEE, 2011, pp. 1–4.

[21] H. Zhao, "An experimental investigation of liquid droplets impinging vertically on a deep liquid pool," Ph.D. dissertation, NTNU, 2009.

[22] G. Taylor, "Studies in electrohydrodynamics. I. The circulation produced in a drop by electrical field," *Proceedings of the Royal Society of London. Series A. Mathematical and Physical Sciences*, vol. 291, no. 1425, pp. 159–166, 1966.